Chapter 1

The Accelerating Universe

Dragan Huterer
Department of Physics, University of Michigan, Ann Arbor, MI 48109

1.1 Introduction and History

In this article we review the discovery of the accelerating universe using type Ia supernovae. We then outline ways in which dark energy – component that causes the acceleration – is phenomenologically described. We finally describe principal cosmological techniques to measure large-scale properties of dark energy. This chapter therefore complements articles by Caldwell and Linder (2010) in this book who describe theoretical understanding (or lack thereof) of the cause for the accelerating universe.

Evidence for the missing component. Inflationary theory [Guth (1981)] explains how tiny quantum-mechanical fluctuations in the early universe could grow to become structures we see on the sky today. One of the factors that motivated inflation is that it predicts that the total energy density relative to the critical value is unity, $\Omega \equiv \rho/\rho_{\rm crit} = 1$. This inflationary prediction convinced many theorists that the universe is precisely flat.

Around the same time that inflation was proposed, a variety of dynamical probes of the large-scale structure in the universe were starting to indicate that the *matter* energy density is much lower than the value needed to make the flat. Perhaps the most specific case was made by the measurements of the clustering of galaxies, which are sensitive to the parameter combination $\Gamma \equiv \Omega_M h$, where Ω_M is the energy density in matter relative to critical, and h is the Hubble constant in units of 100 km/s/Mpc. The measured value at the time was $\Gamma \simeq 0.25$ (with rather large errors). One way to preserve a flat universe was to postulate that the Hubble constant itself was much lower than the measurements indicated ($h \sim 0.7$), so that $\Omega_M = 1$ but $h \sim 0.3$ [Bartlett *et al.* (1995)]. Another possibility was the presence of Einstein's cosmological constant (see the Caldwell article in this book), which was

suggested as far back as 1984 as the possible missing ingredient that could alleviate tension between data and matter-only theoretical predictions [Peebles (1984); Turner *et al.* (1984)] by making the universe older, and allowing flatness with a low value of the matter density.

1.2 Type Ia supernovae and cosmology

The revolutionary discovery of the accelerating universe took place in the late 1990s, but to understand it and its implications, we have to step back a few decades.

Type Ia supernovae. Type Ia supernovae (SN Ia) are explosions seen to distant corners of the universe, and are thought to be cases where a rotating carbon-oxygen white dwarf accretes matter from a companion star, approaches the Chandrasekhar limit, starts thermonuclear burning, and then explodes. The Ia nomenclature refers to spectra of SN Ia, which have no hydrogen, but show a prominent Silicon (Si II) line at 6150Å.

SN Ia had been studied extensively by Fritz Zwicky who also gave them their name [Baade and Zwicky (1934)], and by Walter Baade, who noted that SN Ia have very uniform luminosities [Baade (1938)]. Light from type Ia supernovae brightens and fades over a period of about a month; at its peak flux, a SN Ia can be a sizable fraction of the luminosity of the entire galaxy in which it resides.

Standard candles. It is very difficult to measure *distances* in astronomy. It is relatively easy to measure the angular location of an object; we can also get excellent measurement of the object's redshift z from its spectrum, by observing the shift of known spectral lines due to expansion of the universe ($1 + z = \lambda_{\rm observed}/\lambda_{\rm emitted}$). But the distance measurements traditionally involve empirical — and uncertain — methods: parallax, period-luminosity relation of Cepheids, main-sequence fitting, surface brightness fluctuations, etc. Typically, astronomers construct an unwieldy "distance ladder" to measure distance to a galaxy: they use one of these relations (say, parallaxes – apparent shifts due to Earth's motion around the Sun) to calibrate distances to nearby objects (e.g. variable stars Cepheids), then go from those objects to more distant ones using another relation that works better in that distance regime. In this process the systematic errors add up, making the distance ladder flimsy.

"Standard candles" are hypothetical objects that have a nearly fixed luminosity (that is, fixed intrinsic power that they radiate). Having standard candles would be useful since then we could infer distances to objects just by using the flux-luminosity inverse square law

$$f = \frac{L}{4\pi d_L^2} \tag{1.1}$$

where d_L is the luminosity distance which can be predicted given the object's redshift and contents of the universe (i.e. energy densities of matter and radiation relative to the critical density which makes the universe spatially flat, as well as other components such as radiation). In fact, we don't even need to know the luminosity of the standard candle to be able to infer *relative* distances to objects.

In astronomy, flux is often expressed in terms of apparent magnitude – a logarithmic measure of flux, and luminosity is related to the absolute magnitude of the object. So, in astronomical units, Eq. (1.1) reads

$$m - M = 5 \log_{10} \left(\frac{d_L}{10\,\mathrm{pc}} \right) \tag{1.2}$$

where the quantity on the left-hand side is also known as the *distance modulus*. For an object that is 10 parsecs away, the distance modulus is zero. For a standard candle, the absolute magnitude M (or, equivalently, luminosity L) is known to be approximately the same for each object. Therefore, measurements of the apparent magnitude to each object provide information about the luminosity distance, and thus the makeup of the universe.

Finding SN. The fact that SN Ia can potentially be used as a standard candle has been realized long ago, at least as far back as the 1970s [Kowal (1968); Colgate (1979)]. However, a major problem is to find a method to schedule telescopes to discover SN before they happen. If we point a telescope at a galaxy and wait for the SN to go off, we will wait several hundred years. There had been a program in the 1980s to find supernovae [Norgaard-Nielsen *et al.* (1989)] but, partly due to inadequate technology and equipment available at the time, it discovered only one SN, and after the peak of the light-curve.

The first major breakthrough came in the 1990s when two teams of SN researchers Supernova Cosmology Project (SCP; led by Saul Perlmutter and organized in the late 1980s) and High-z Supernova Search Team (Highz; organized in the mid 1990s and led, at the time, by Brian Schmidt) developed an efficient approach to use world's most powerful telescopes working in concert to discover and follow up high-redshift SN, and thus complement the existing efforts at lower redshift led by the Calán/Tololo collaboration [Hamuy *et al.* (1996)]. These teams had been able to essentially guarantee that they would find batches of SN in each run. [For popular reviews of these exciting developments, see Kirshner (2002) and Perlmutter and Schmidt (2003).]

The second breakthrough came in 1993 by Mark Phillips, astronomer working in Chile [Phillips (1993)]. He noticed that the SN luminosity – or absolute magnitude – is correlated with the decay time of SN light curve. Phillips considered the quantity Δm_{15}, the attenuation of the flux of SN between the light maximum and 15 days past the maximum. He found that Δm_{15} is strongly correlated with the intrinsic brightness of SN; see the left panel of Fig. 1.1. The "Phillips relation" roughly goes as

Broader is brighter.

In other words, supernovae with broader light-curves have a larger intrinsic luminosity. One way to quantify this relation is to use a "stretch" factor which is a (calibration) parameter that measures width of a light curve [Perlmutter *et al.* (1999)]; see the right panel of Fig. 1.1. By applying the correction based upon the Phillips relation, astronomers found that the intrinsic dispersion of SN, which is of order ~ 0.5 magnitudes, can be brought down to $\delta m \sim 0.2$ magnitudes once we correct each SN luminosity using its stretch factor. Note that the final dispersion in magnitudes corresponds to the error in distance of $\delta d_L/d_L = (\ln(10)/5)\,\delta m \simeq 0.5\,\delta m \sim 0.1$. The Phillips relation was the second key ingredient that enabled SN Ia to achieve precision needed to probe contents of the universe accurately.

The third key invention was the development of techniques to correct SN magnitudes for dimming by dust, or 'extinction', out of multi-color observation of SN light [Riess *et al.* (1996a,b)]. Such corrections are an important part of SN cosmology to this day [Jha *et al.* (2007); Guy *et al.* (2007); Conley *et al.* (2008)].

Finally, the fourth and perhaps most important ingredient for the discovery of dark energy was development and application of charge-coupled devices (CCDs) in observational astronomy. Both teams of SN hunters used the CCDs, which had originally been installed at telescopes at Kitt Peak and Cerro Tololo [Kirshner (2009)].

Some of the early results came out in the period of 1995-1997; however these results were based on a handful of high-redshift SN and had large errors (e.g. [Perlmutter *et al.* (1997); Garnavich *et al.* (1998); Perlmutter *et al.* (1998)]).

The discovery of dark energy. The definitive results, based on $\sim$ 50 SN by either team that combined the nearby sample previously observed by the Calán/Tololo collaboration and the newly acquired and crucial sample of high-redshift SN, came out soon thereafter [Riess *et al.* (1998); Perlmutter *et al.* (1999)]. The results of the two teams agreed, and indicated that more distant SN are dimmer than would be expected in a matter-only universe; see Fig. 1.2. In other words, the universe's expansion rate is speeding up, contrary to expectation from the matter-dominated universe with *any* amount of matter and regardless of curvature.

Phrased yet differently, the data indicate universe that is accelerating – that is presence of a new component with strongly negative pressure. This can easily be seen from the *acceleration equation*, which is one of Einstein's equations applied to the case of the homogeneous universe

$$\frac{\ddot{a}}{a} = -\frac{4\pi G}{3}(\rho + 3p) = -\frac{4\pi G}{3}(\rho_M + \rho_{\rm DE} + 3p_{\rm DE}) \tag{1.3}$$

where ρ and p are the energy density and pressure of components in the universe, assuming they are matter and a new component we call dark energy (radiation is negligible relative to matter at redshifts much less than $\sim 10^3$, and the pressure of matter is always negligible). If the universe is accelerating, then $\ddot{a} > 0$, and the only

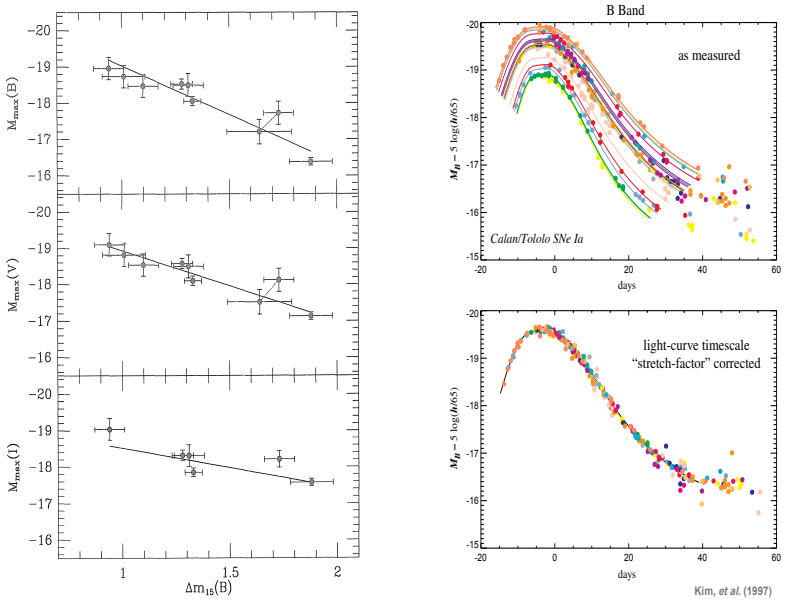

Fig. 1.1 *Left panel:* Phillips relation, from his 1993 paper. The (apparent) magnitude of type Ia supernovae is correlated with Δm_{15}, the decay of the light curve 15 days after the maximum. *Right panel:* light curves of a sample of SN Ia before correction for stretch (essentially, the Phillips relation; top), and after (bottom); adopted from Kim (2008).

way it can be is if the *pressure of the new component is strongly negative*. Phrased in terms of equation of state, $w \equiv p_{\rm DE}/\rho_{\rm DE} < -1/3$ regardless of the density of matter ρ_M.

The discovery of the accelerating universe with supernovae was a watershed event in modern cosmology, and the aforementioned two discovery papers are among the most cited physics papers of all time. This component that makes the universe accelerate was soon named "dark energy" by the theoretical cosmologist Michael Turner [Huterer and Turner (1999)].

The SN data are illustrated in Fig. 1.2, where upwards of 500 SN measurements from the Union2 compilation [Amanullah *et al.* (2010)] have been binned in redshift. The blue line shows a model that fits the data, where acceleration happens at late epochs in the history of the universe (i.e. starting a few billion years ago, and billions of years after the Big Bang). For illustration, we also show three representative matter-only models in green, with open, closed and flat geometry, neither of which fits the data well. Finally, the red curve shows a model that always exhibits acceleration, and it too does not fit the SN data which show a characteristic "turnover" in the magnitude vs. redshift plot.

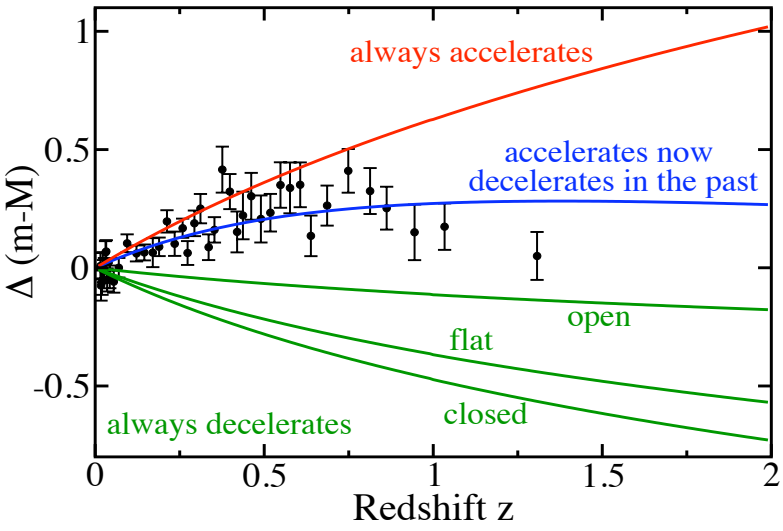

Fig. 1.2 Evidence for transition from deceleration in the past to acceleration today. The blue line shows a model that fits the data, where acceleration happens at late epochs in the history of the universe (i.e. starting a few billion years ago, and billions of years after the Big Bang). For illustration, we also show three representative matter-only models in green, with open, closed and flat geometry. Finally, the red curve shows a model that always exhibits acceleration, and it too does not fit the SN data which show a characteristic "turnover" in the magnitude vs. redshift plot. The plot uses binned data from the Union2 compilation [Amanullah *et al.* (2010)] containing 557 SN.

Observable and inferred quantities with SN Ia. The luminosity distance d_L is related to the cosmological parameters via

$$d_L = (1+z)\frac{H_0^{-1}}{\sqrt{\Omega_K}}\,\sinh\left[\sqrt{\Omega_K}\int_0^z \frac{dz'}{\sqrt{\Omega_M(1+z)^3+\Omega_{\rm DE}(1+z)^{3(1+w)}+\Omega_R(1+z)^4+\Omega_K(1+z)^2}}\right] \tag{1.4}$$

where the key term in this expression featuring $\sinh(x)$ for $\Omega_K > 0$ (open universe) effectively turns into $\sin(x)$ (closed universe; $\Omega_K < 0$) or just x (flat universe; $\Omega_K = 0$). Here Ω_M, Ω_R, and $\Omega_{\rm DE}$ are the energy densities of matter (visible plus dark), radiation (mainly cosmic microwave background (CMB) photons), and dark energy relative to critical density, and $\Omega_K = 1 - \Omega_M - \Omega_R - \Omega_{\rm DE}$.

Now Eq. (1.2) can be rewritten as

$$m \equiv 5\log_{10}(H_0 d_L) + \mathcal{M} \tag{1.5}$$

where the "script-M" factor is defined as

$$\mathcal{M} \equiv M - 5\log_{10}\left(\frac{H_0}{\rm Mpc^{-1}}\right) + 25. \tag{1.6}$$

Note that $\mathcal{M}$ is a dummy parameter that captures *two* uncertain quantities: the absolute magnitude (i.e. intrinsic luminosity) of a supernova, M, and the Hub-

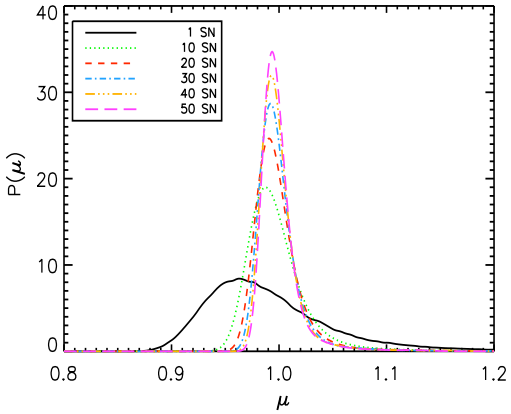

Fig. 1.3 Magnification distribution for lensing of a supernova at $z = 1.5$ in the usual ΛCDM cosmology (black curve). Other curves show how the distribution both narrows and becomes more gaussian as we average over more SN. Adopted from Holz and Linder (2005).

ble constant H_0. We typically do not know $\mathcal{M}$, and we need to marginalize (i.e. integrate) over all values of this parameter in the cosmological analysis.

The situation is now clear: astronomers measure m, which is inferred, for example, from the flux at the peak of the light curve. Then they measure the redshift of SN host galaxy. With the sufficient number of SN measurements, they can marginalize over the parameter $\mathcal{M}$ and be left with, effectively, measurements of luminosity distance vs. redshift. A plot of either $m(z)$ or $d_L(z)$ is called the Hubble diagram.

These results have been greatly strengthened since, with many hundreds of SN Ia currently indicating same results, but with smaller errors, compared to the original 1998-99 papers [Knop *et al.* (2003); Riess *et al.* (2004); Astier *et al.* (2006); Riess *et al.* (2007); Wood-Vasey *et al.* (2007); Kessler *et al.* (2009); Hicken *et al.* (2009); Amanullah *et al.* (2010)]. Meanwhile, other cosmological probes have come in with results confirming the SN results (see the right panel of Fig. 1.4).

Systematic errors. Systematic errors may creep up in SN observations, and stand in the way of making SN Ia a more precise tool of cosmology. Here we list a few prominent sources of error, and ways in which they are controlled:

- Extinction: is it possible that SN appear dimmer simply because of extinction by dust particles scattered between us and distant SN? Fortunately there are ways to stringently control (and correct for) extinction, by observing SN in different wavelength bands. But also, if extinction were to be responsible for the appearance of dimming, then we would expect more distant SN to appear uniformly more dim. Moreover, a "turnover" in the SN Hubble diagram has been clearly observed (e.g. Riess *et al.* (2004)) indicating that the universe is matter dominated at high z. The turnover

cannot easily be explained by extinction.

- Evolution: is it possible that SN evolve, so that we are seeing a different population at higher redshift that is intrinsically dimmer (violating the assumption of a standard candle)? SN Ia do not own a "cosmic clock"; rather, they respond to their local environment, in addition to being ruled by the physics of accretion/explosion. So, by observing various signatures, in particular in SN spectra, researchers can identify local environmental conditions, and even go so far to compare only like-to-like SN (resulting, potentially, in several Hubble diagrams, one for each subspecies). First such comparisons have been made recently.
- Typing: is it possible that non-Ia supernovae have crept in the samples used for dark energy analysis? This question is rather easy to answer, as SN Ia possess characteristic spectral lines which uniquely identify these SN. Accurate typing, however, becomes more challenging for SN surveys which cannot afford to take spectra of all SN; upcoming and future imaging surveys such as the Dark Energy Survey (DES) or Large Synoptic Survey Telescope (LSST) are examples. For those surveys, one will have to apply sophisticated tests based on photometric information alone to establish whether or not a given supernova is type Ia.
- K-corrections: As SN Ia are observed at larger and larger redshifts, their light is shifted to longer wavelengths. Since astronomical observations are normally made in fixed band passes on Earth, corrections need to be applied to account for the differences caused by the spectrum shifting within these band passes, and error in these corrections needs to be tightly controlled.
- Gravitational lensing: distant SN are gravitationally lensed by matter along the line of sight, making them magnified or demagnified, and thus appearing brighter or dimmer. The lensing effect goes roughly as z^2 and is non-negligible only for high-z SN; $z \gtrsim 1.2$. The *mean* magnification is zero (owing to a theorem that the total light is conserved), but the distribution is skewed, meaning that most SN get demagnified but occasional ones get strongly magnified. The way to protect against biases due to gravitational lensing is to seek "safety in numbers" [Holz and Linder (2005)]: simply put, if we collect enough SN at any given redshift (in practice, ~ 50 SN per $\Delta z = 0.1$), the effects of gravitational lensing will average down to near zero; see Fig. 1.3.

At the present time the SN systematic errors are well controlled, and are comparable to the statistical errors. The factor that gives undisputed credence to the result that the universe is accelerating, however, is confirmation with the galaxy clustering (the baryon acoustic oscillations, to be described later in this article), and the CMB constraints; see Fig. 1.4. In fact, even if one completely drops the SN constraints from the analysis, the combination of the galaxy clustering and the

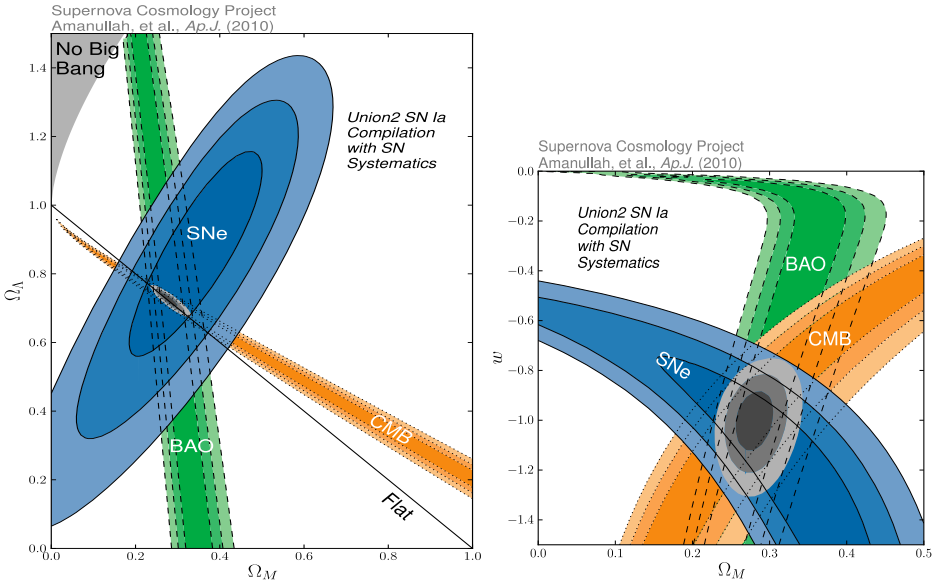

Fig. 1.4 *Left panel*: Constraints upon $\Omega_{\rm M}$ and Ω_Λ in the consensus model using baryon acoustic oscillation (BAO), CMB, and SN measurements. *Right panel*: Constraints upon $\Omega_{\rm M}$ and constant w in the fiducial dark energy model using the same data sets. From Amanullah *et al.* (2010).

CMB firmly points to the existence of dark energy!

1.3 Parametrizations of dark energy

Introduction. The absence of a consensus model for cosmic acceleration presents a challenge in trying to connect theory with observations. For dark energy, the equation-of-state parameter w provides a useful phenomenological description; because it is the ratio of pressure to energy density, it is also closely connected to the underlying physics. On the practical side, determining a free function is more difficult than measuring parameters. We now review a variety of formalisms that have been used to describe and constrain dark energy.

First, let us recall some basics. From continuity equation, $\dot{\rho} + 3H(p + \rho) = 0$, we can calculate the dark energy density as a function of redshift for an arbitrary equation of state $w(z)$

$$\frac{\rho_{\rm DE}(z)}{\rho_{\rm DE,0}} = \exp\left(3\int_0^z (1 + w(z'))d\ln(1 + z')\right). \tag{1.7}$$

Parametrizations. The simplest parameterization of dark energy is

$$w = \text{const.} \tag{1.8}$$

This form fully describes vacuum energy ($w = -1$) or topological defects ($w = -N/3$ with N an integer dimension of the defect – 0 for monopoles, 1 for strings, 2 for domain walls). Together with $\Omega_{\rm DE}$ and $\Omega_{\rm M}$, w provides a 3-parameter description of the dark-energy sector (2 parameters if flatness is assumed). However, it does not describe scalar field or modified gravity models which generically have a time-varying w.

A number of two-parameter descriptions of w have been explored in the literature, e.g., $w(z) = w_0 + w'z$ [Cooray and Huterer (1999)]. For low redshift they are all essentially equivalent, but for large z, some lead to unrealistic behavior, e.g., $w \ll -1$ or $\gg 1$. The parametrization [Linder (2003)]

$$w(a) = w_0 + w_a(1-a) = w_0 + w_a \frac{z}{1+z} \tag{1.9}$$

where $a = 1/(1+z)$ is the scale factor, avoids this problem, fits many scalar field and some modified gravity behaviors, and leads to the most commonly used description of dark energy, namely $(\Omega_{\rm DE}, \Omega_{\rm M}, w_0, w_a)$. The energy density is then

$$\frac{\rho_{\rm DE}(a)}{\rho_{\rm DE,0}} = a^{-3(1+w_0+w_a)} e^{-3(1-a)w_a}. \tag{1.10}$$

More general expressions have been proposed. However one problem with introducing more parameters is that additional parameters make the equation of state very difficult to measure, while the parametrizations are still *ad hoc* and not well motivated from either theory or measurements' point of view.

Finally, it is useful to mention one simple way to elucidate redshift where the measurement accuracy of the equation of state, for a given survey is highest. Two-parameter descriptions of $w(z)$ that are linear in the parameters entail the existence of a "pivot" redshift z_p at which the measurements of the two parameters are uncorrelated and the error in $w_p \equiv w(z_p)$ reaches a minimum; see the left panel of Fig. 1.5. Writing the equation of state in Eq. (1.9) in the form

$$w(a) = w_p + (a_p - a)w_a \tag{1.11}$$

it is easy to translate constraints from the (w_0, w_a) to (w_p, w_a) parametrization, as well as determine a_p (or z_p), for any particular data set. This is useful, as measurements of the equation of state at the pivot point might provide most useful information in ruling out models (e.g. ruling out $w = -1$).

Direct reconstruction. Another approach is to directly invert the redshift-distance relation $r(z)$ measured from SN data to obtain the redshift dependence of $w(z)$ in terms of the first and second derivatives of the comoving distance [Huterer and Turner (1999); Nakamura and Chiba (1999); Starobinsky (1998)],

$$1 + w(z) = \frac{1+z}{3} \, \frac{3H_0^2\Omega_{\rm M}(1+z)^2 + 2(d^2r/dz^2)/(dr/dz)^3}{H_0^2\Omega_{\rm M}(1+z)^3 - (dr/dz)^{-2}} \ . \tag{1.12}$$

Assuming that dark energy is due to a single rolling scalar field, the scalar potential $V(\phi)$ can also be reconstructed. Others have suggested reconstructing the dark energy density [Wang and Mukherjee (2004); Wang and Tegmark (2005)]

$$\rho_{\rm DE}(z) = \frac{3}{8\pi G}\left[\frac{1}{(dr/dz)^2} - \Omega_{\rm M} H_0^2 (1+z)^3\right] . \tag{1.13}$$

Direct reconstruction is the only approach that is truly model-independent. However, it comes at a price – taking derivatives of noisy data. In practice, one must fit the distance data with a smooth function, and the fitting process introduces systematic biases. While a variety of methods have been pursued [Huterer and Turner (2001); Weller and Albrecht (2002)], it appears that direct reconstruction is too challenging and not robust even with SN Ia data of excellent quality (though see Holsclaw *et al.* (2010)). And while the reconstruction of $\rho_{\rm DE}(z)$ is easier since it involves only first derivatives of distance, $w(z)$ is more useful a quantity since it contains more information about the nature of dark energy than $\rho_{\rm DE}(z)$. [For a review of dark energy reconstruction methods, see Sahni and Starobinsky (2006).]

Principal components. The cosmological function that we are trying to determine — $w(z)$, $\rho_{\rm DE}(z)$, or $H(z)$ — can be expanded in terms of principal components, a set of functions that are uncorrelated and orthogonal by construction [Huterer and Starkman (2003)]. In this approach, the data determine which components are measured best.

For example, suppose we parametrize $w(z)$ in terms of piecewise constant values w_i $(i = 1, \ldots, N)$, each defined over a small redshift range $(z_i,\ z_i + \Delta z)$. In the limit of small Δz this recovers the shape of an arbitrary dark energy history (in practice, $N \gtrsim 20$ is sufficient), but the estimates of the w_i from a given dark energy probe will be very noisy. Principal Component Analysis extracts from those noisy estimates the best-measured features of $w(z)$. We find the eigenvectors $e_i(z)$ of the inverse covariance matrix for the parameters w_i and the corresponding eigenvalues λ_i. The equation-of-state parameter is then expressed as

$$1 + w(z) = \sum_{i=1}^{N} \alpha_i\, e_i(z) , \tag{1.14}$$

where the $e_i(z)$ are the principal components. The coefficients α_i, which can be computed via the orthonormality condition

$$\alpha_i = \int (1 + w(z)) e_i(z) dz \tag{1.15}$$

are each determined with an accuracy $1/\sqrt{\lambda_i}$. Several of these components are shown for a future SN survey in the right panel of Fig. 1.5, while measurements of the first six PCs of the equation of state from the current (and predictions for future) data are shown in Fig. 1.6.

There are multiple advantages of using the PCs of dark energy (of either the equation of state $w(z)$, or of $\rho_{\rm DE}(z)$ or $H(z)$):

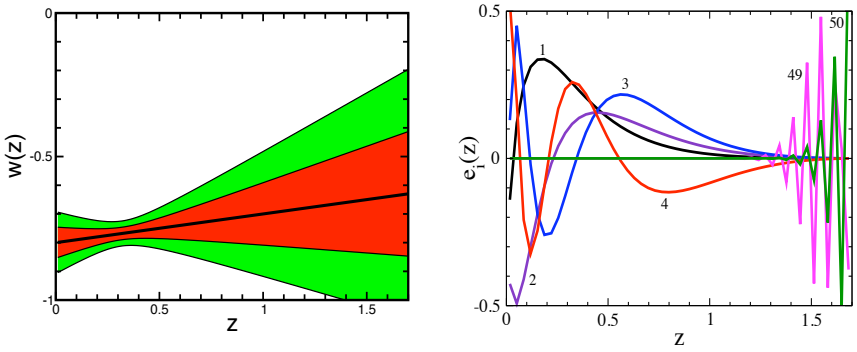

Fig. 1.5 *Left panel:* Example of forecast constraints on $w(z)$, assuming $w(z) = w_0 + w'z$. The "pivot" redshift, $z_p \simeq 0.3$, is where $w(z)$ is best determined. Adopted from Huterer and Turner (2001). *Right panel:* The four best-determined (labelled 1-4) and two worst-determined (labelled $49, 50$) principal components of $w(z)$ for a future SN Ia survey such as SNAP, with several thousand SN in the redshift range $z = 0$ to $z = 1.7$. Adopted from Huterer and Starkman (2003).

- The method is as close to "model independent" as one can realistically get;
- Data tells us what we measure and how well; there are no arbitrary parametrizations imposed;
- One can use this approach to design a survey that is most sensitive to the dark energy equation-of-state parameter in some specific redshift interval...
- ...or to study how many independent parameters are measured well by a combination of cosmological probes (i.e. how many PCs have $\sigma(\alpha_i)$ or $\sigma(\alpha_i)/\alpha_i$ less than some threshold value [de Putter and Linder (2008)]).

There are a variety of useful extensions of this method, including uncorrelated measurements of the equation-of-state parameters in redshift intervals [Huterer and Cooray (2005)].

Figures of Merit. We finally discuss the so-called figures of merit (FoMs) for dark energy experiments. A FoM is a number, or collection of numbers, that serve as simple and quantifiable metrics by which to evaluate the accuracy of constraints on dark energy parameters from current and proposed experiments. For example, marginalized accuracy in the (constant) equation of state, w, could serve as a figure of merit – since a large FoM is "good", we could simply define FoM $= 1/\sigma_w$, or $1/\sigma_w^m$ where m is some positive power.

The most commonly discussed figure of merit is that proposed by the Dark Energy Task Force (Albrecht *et al.* (2006), though this proposal goes back to Huterer and Turner (2001)), which is essentially inverse area in the w_0–w_a plane. For uncorrelated w_0 and w_a this would be $\propto 1/(\sigma_{w_0} \times \sigma_{w_a})$; because the two are typically

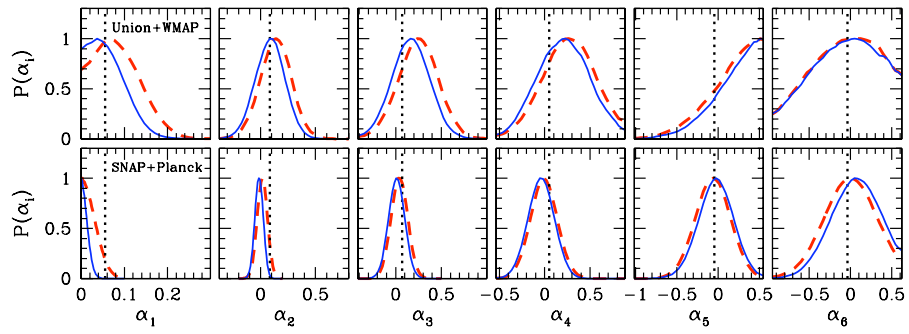

Fig. 1.6 Marginalized 1D posterior distributions for the first 6 PCs of flat (solid blue curves) and nonflat (dashed red curves) quintessence models. Top row: *current* Union+WMAP data; note that all PCs are consistent with $\alpha_i = 0$ (that is, $w(z) = -1$) except perhaps the fifth one. Bottom row: forecasts for *future* SNAP+Planck *assuming* a realization of the data with $\alpha_i = 0$. Vertical dotted lines show the predictions of an example quintessence model. Adopted from Mortonson *et al.* (2010).

correlated, the FoM can be defined as

$$\mathrm{FoM}^{(w_0-w_a)} \equiv (\det \mathbf{C})^{-1/2} \approx \frac{6.17\pi}{A_{95}}, \tag{1.16}$$

where $\mathbf{C}$ is the 2×2 covariance matrix in (w_0, w_a) after marginalizing over all other parameters, and A_{95} is the area of the 95.4% CL region in the w_0–w_a plane. Note that the constant of proportionality is not important, since typically we compare the FoM from different surveys, and the constant disappears when we take the ratio.

While the standard "DETF FoM" defined in Eq. (1.16) keeps some information about the dynamics of DE (that is, the time variation of $w(z)$), several other general FoMs have been proposed. For example, Mortonson *et al.* (2010) proposed taking the FoM to be inversely proportional to the volume of the n-dimensional ellipsoid in the space of principal component parameters

$$\mathrm{FoM}_n^{(\mathrm{PC})} \equiv \left(\frac{\det \mathbf{C}_n}{\det \mathbf{C}_n^{(\mathrm{prior})}}\right)^{-1/2}, \tag{1.17}$$

where the prior covariance matrix is again unimportant since it would cancel in the comparison of ratios of the FoMs. Fig. 1.10, near the end of this Chapter, illustrates this FoM for current and future surveys.

1.4 Other probes of dark energy

In addition to type Ia supernovae, there are several other important probes of dark energy. These probes operate using very different physics, and have very different systematic errors.

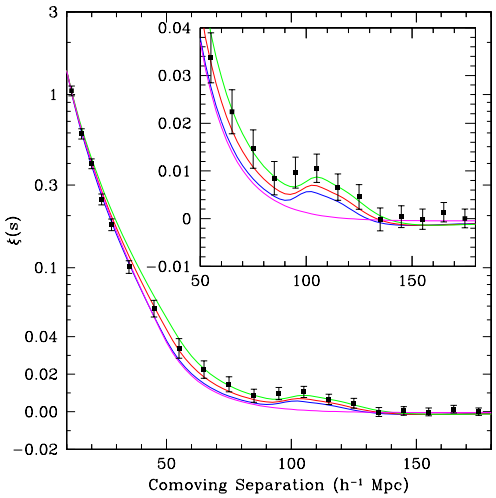

Fig. 1.7 Detection of the baryon acoustic peak in the clustering of luminous red galaxies in the SDSS [Eisenstein *et al.* (2005)]. Shown is the two-point galaxy correlation function in redshift space; inset shows an expanded view with a linear vertical axis. Curves correspond to ΛCDM predictions for $\Omega_{\rm M}h^2 = 0.12$ (green), 0.13 (red), and 0.14 (blue). Magenta curve shows a ΛCDM model without BAO.

The principal probes, in addition to SN Ia, are baryon acoustic oscillations, weak gravitational lensing, and galaxy cluster abundance. We will now discuss each of those in turn. Additionally, there are secondary probes of dark energy — ones that might be useful for DE, but are currently not as well developed as the primary probes. We will discuss these briefly as well.

Baryon acoustic oscillations (BAO). BAO refers to the signature of acoustic oscillations which are imprinted into the present-day correlations of galaxies by baryonic physics at the epoch of recombination (for a popular review, see Eisenstein (2005)). Measurements of the length scale characteristic of these oscillations, roughly $100\,{\rm h}^{-1}$Mpc comoving, enable inferring the angular diameter distance out to galaxies probed in a survey, and thus a robust way to measure the energy contents of the universe.

Note that the power spectrum of density perturbations in dark matter, $P(k)$, is mainly sensitive to the density in matter (relative to critical), Ω_M. If we assume a flat universe (either motivated by the inflationary "prior", or by recent data), then $\Omega_{\rm DE} = 1 - \Omega_M$ and measurements of the broad-band shape of the power spectrum can get the dark energy density, but not the equation of state w.

However, the small ($\sim 10\%$) *oscillations* in the power spectrum provide much more information about DE. The BAO data determine the ratio of the sound horizon at last scattering to the quantity $D_V(z) \equiv [z\,r^2(z)/H(z)]^{1/3}$ at the measured redshift; given that the sound horizon is independently determined rather accu-

rately, the BAO approximately provides measurement of distance to the redshift where the galaxies reside. For example, Percival *et al.* (2010) analyze combined data from 2-degree Field Galaxy Redshift Survey and the Sloan Digital Sky Survey which measure the clustering at mean redshifts $z = 0.2$ and $z = 0.35$ respectively.

Key to successful application of baryon acoustic oscillations are redshift measurements of galaxies in the sample. We need the galaxy redshifts in order to know where to "put them" in three dimensions, and thus to reconstruct the precise length scale at which the slight excess of clustering occurs. Another systematic that needs to be understood is the bias of galaxies in the sample (whose clustering we measure) to the underlying dark matter (whose clustering we can predict); if the bias has scale-dependent features on scales of $\sim 100\,\mathrm{Mpc}$, then the systematic errors creep in. Future surveys that plan to utilize this method typically propose measuring redshifts of millions of galaxies, and the goal is to go deep ($z \sim 1$, and beyond) and have wide angular coverage as well.

Let us finally say a few words about the measured quantity, the power spectrum. In the dimensionless form, it is given by

$$\Delta^2(k) \equiv \frac{k^3 P(k)}{2\pi^2} = A\,\frac{4}{25}\frac{1}{\Omega_M^2}\left(\frac{k}{k_{\rm piv}}\right)^{n-1}\left(\frac{k}{H_0}\right)^4 D(z)^2\,T^2(k)\,T_{\rm nl}(k)\,, \qquad (1.18)$$

where A is the normalization of the power spectrum (for the concordance cosmology, $A \simeq 2.4 \times 10^{-9}$), $k_{\rm piv}$ is the "pivot" around which we compute the spectral index n ($k_{\rm piv} = 0.002\,\mathrm{Mpc}^{-1}$ is often used); $D(z)$ is the linear growth of perturbations normalized to unity today; $T(k)$ is the transfer function that describes evolution of fluctuations inside the horizon and across the matter-radiation transition epoch and which encodes the BAOs; $T_{\rm nl}$ is a prescription for the *nonlinear* power spectrum which is relevant at small scales (e.g. $k \gtrsim 0.2\,\mathrm{h\,Mpc}^{-1}$ today). Notice that $\Delta^2 \propto k^{n+3}$, and thus $P(k) \propto k^n$, with $n \simeq 1$, was predicted by Harrison, Zeldovich and Peebles in the late 1960s; this was a decade before inflation was proposed, and about three decades before measurements confirmed that $n \simeq 1$!

Weak gravitational lensing. The gravitational bending of light by structures in the Universe distorts or shears images of distant galaxies; see the left panel of Fig. 1.8. This distortion allows the distribution of dark matter and its evolution with time to be measured, thereby probing the influence of dark energy on the growth of structure (for a detailed review, see e.g. Bartelmann and Schneider (2001); for brief reviews, see Hoekstra and Jain (2008) and Huterer (2010)).

Gravitational lensing produces distortions of images of background galaxies. These distortions can be described as mapping between the source plane (S) and image plane (I)

$$\delta x_i^S = A_{ij}\delta x_j^I\,, \qquad (1.19)$$

where $\delta\mathbf{x}$ are the displacement vectors in the two planes and A is the distortion matrix

$$A = \begin{pmatrix} 1-\kappa-\gamma_1 & -\gamma_2 \\ -\gamma_2 & 1-\kappa+\gamma_1 \end{pmatrix}. \qquad (1.20)$$

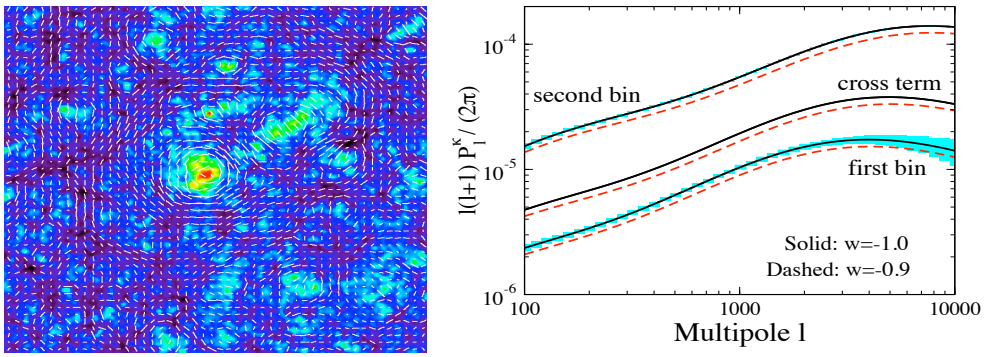

Fig. 1.8 *Left panel:* Cosmic shear field (white ticks) superimposed on the projected mass distribution from a cosmological N-body simulation: overdense regions are bright, underdense regions are dark. Note how the shear field is correlated with the foreground mass distribution. Figure courtesy of T. Hamana. *Right panel:* Cosmic shear angular power spectrum and statistical errors expected for LSST for $w = -1$ and -0.9. For illustration, results are shown for source galaxies in two broad redshift bins, $z_s = 0 - 1$ (first bin) and $z_s = 1 - 3$ (second bin); the cross-power spectrum between the two bins (cross term) is shown without the statistical errors.

The deformation is described by the convergence κ and complex shear (γ_1, γ_2); the total shear is defined as $|\gamma| = \sqrt{\gamma_1^2 + \gamma_2^2}$. We are interested in the weak lensing limit, where κ, $|\gamma| \ll 1$. Magnification can be expressed in terms of κ and $\gamma_{1,2}$ as

$$\mu = \frac{1}{|1-\kappa|^2 - |\gamma|^2} \approx 1 + 2\kappa + O(\kappa^2, \gamma^2), \tag{1.21}$$

where the second approximate relation holds in the weak lensing limit.

We can theoretically predict convergence and shear, given a sample of sources with known redshift distribution and cosmological parameter values. The convergence in any particular direction on the sky $\hat{\mathbf{n}}$ is given by the integral along the line-of-sight

$$\kappa(\hat{\mathbf{n}}, \chi) = \int_0^\chi W(\chi')\, \delta(\chi')\, d\chi' \,, \tag{1.22}$$

where δ is the perturbation in matter energy density and $W(\chi)$ is the geometric weight function describing the lensing efficiency of foreground galaxies. The most efficient lenses lie about half-way between us and the source galaxies whose shapes we measure.

The statistical signal due to gravitational lensing by large-scale structure is termed "cosmic shear." The cosmic shear field at a point in the sky is estimated by locally averaging the shapes of large numbers of distant galaxies. The primary statistical measure of the cosmic shear is the shear angular power spectrum measured as a function of source galaxy redshift z_s. (Additional information is obtained by measuring the correlations between shears at different redshifts or with foreground lensing galaxies.)

The convergence can be transformed into multipole space $\kappa_{lm} = \int d\hat{\mathbf{n}}\, \kappa(\hat{\mathbf{n}}, \chi)\, Y^*_{lm}(\hat{\mathbf{n}})$, and the power spectrum is defined as the two-point correlation function (of convergence, in this case) $\langle \kappa_{\ell m} \kappa_{\ell' m'} \rangle = \delta_{\ell\ell'}\, \delta_{mm'}\, P^\kappa_\ell$. The angular power spectrum is

$$P^\gamma_\ell(z_s) \simeq P^\kappa_\ell(z_s) = \int_0^{z_s} \frac{dz}{H(z) d_A^2(z)} W(z)^2 P\left(k = \frac{\ell}{d_A(z)}; z\right), \tag{1.23}$$

where ℓ denotes the angular multipole, $d_A(z) = (1+z)^{-2} d_L(z)$ is the angular diameter distance, the weight function $W(z)$ is the efficiency for lensing a population of source galaxies and is determined by the distance distributions of the source and lens galaxies, and $P(k, z)$ is the usual power spectrum of density perturbations. Notice the integral along the line of sight: essentially, weak lensing projects the density fluctuations between us and the galaxies whose shear we measure.

The dark-energy sensitivity of the shear angular power spectrum comes from two factors:

- *geometry* – the Hubble parameter, the angular-diameter distance, and the weight function $W(z)$; and
- *growth of structure* – through the redshift evolution of the power spectrum $P(k)$ (or more precisely, from the function $D(z)$ in Eq. (1.18)).

The *three*-point correlation function of cosmic shear is also sensitive to dark energy, and provides important complementary information about dark energy (e.g. Takada and Jain (2004)).

The statistical uncertainty in measuring the shear power spectrum on large scales is

$$\Delta P^\gamma_\ell = \sqrt{\frac{2}{(2\ell+1) f_{\rm sky}}} \left[P^\gamma_\ell + \frac{\sigma^2(\gamma_i)}{n_{\rm eff}} \right] \quad , \tag{1.24}$$

where $f_{\rm sky}$ is the fraction of sky area covered by the survey ($f_{\rm sky} = 0.5$ for half-sky, etc), $\sigma^2(\gamma_i)$ is the variance in a single component of the (two-component) shear (this number is ~ 0.2 for typical measurements), and $n_{\rm eff}$ is the effective number density per steradian of galaxies with well-measured shapes. The first term in brackets dominates on large scales, and comes from sample variance (also known as *cosmic variance*) due to the fact that only a finite number of samples of structures are available in our universe. The second term dominates on small scales, and represents the shot-noise from the variance in galaxy ellipticities ("shape noise") combined with a finite number of galaxies, hence the inverse proportionality to $n_{\rm eff}$.

The principal systematic errors in weak lensing measurements come from the limitations in measuring galaxy shapes accurately. There are also systematic uncertainties due to limited knowledge of the redshifts of source galaxies: because taking spectroscopic redshifts of most source galaxies will be impossible (they number in many millions), one has to rely to approximate photometric redshift techniques,

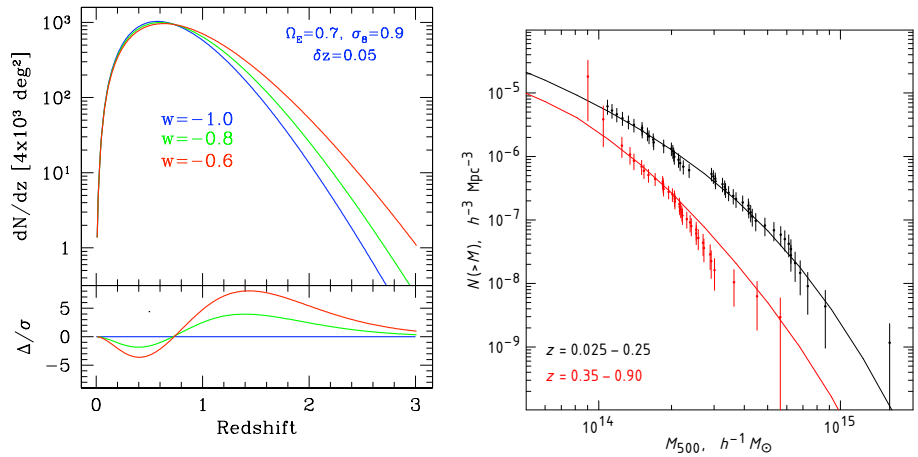

Fig. 1.9 *Left panel:* Predicted cluster counts for a survey covering 4,000 sq. deg. that is sensitive to halos more massive than $2 \times 10^{14} M_\odot$, for 3 flat cosmological models with fixed $\Omega_{\rm M} = 0.3$ and $\sigma_8 = 0.9$. Lower panel shows fractional differences between the models in terms of the estimated Poisson errors. From Mohr (2005). *Right panel:* Measured mass function – $n(z, M_{\rm min}(z))$ – in our notation – from the 400 square degree survey of ROSAT clusters followed up by Chandra. Adopted from Vikhlinin *et al.* (2009).

where one gets redshift information from multiple-wavelength (i.e. multi-color) observations.

The right panel of Fig. 1.8 shows the dependence on the dark energy of the shear power spectrum and an indication of the statistical errors expected for a survey such as LSST, assuming a survey area of 15,000 sq. deg. and effective source galaxy density of $n_{\rm eff} = 30$ galaxies per sq. arcmin, and divided into two radial slices. Current surveys cover a more modest ~ 100 square degrees, with a comparable or slightly lower galaxy density. Note that the proportionality of errors to $f_{\rm sky}^{-1/2}$ means that large sky coverage is at a premium.

Clusters of galaxies. Galaxy clusters are the largest virialized objects in the Universe. Therefore, not only can they be observed, but also their number density can be *predicted* quite reliably, both analytically and from numerical simulations. Comparing these predictions to measurements from the large-area cluster surveys that extend to high redshift ($z \gtrsim 1$) can provide precise constraints on the cosmic expansion history.

The absolute number of clusters in a survey of solid angle $\Omega_{\rm survey}$ centered at redshift z and in the shell of thickness Δz is given by

$$N(z, \Delta z) = \Omega_{\rm survey} \int_{z-\Delta z/2}^{z+\Delta z/2} n(z, M_{\rm min}(z)) \, \frac{dV(z)}{d\Omega \, dz} \, dz, \qquad (1.25)$$

where $M_{\rm min}$ is the minimal mass of clusters in the survey (usually of order $10^{14} M_\odot$). Note that knowledge of the minimal mass is extremely important, since the mass

function $n(z, M_{\rm min}(z))$ is exponentially decreasing with M, so that most of the contribution comes from a small range of masses just above $M_{\rm min}$. The mass function is key to theoretical predictions, and it is usually obtained from a combination of analytic and numerical results; the original mass function used in cosmology is the 36-year old Press-Schechter mass function [Press and Schechter (1974)], and the more recent work provides fitting functions to simulations' results that are accurate to several percent [Tinker *et al.* (2008)]. Furthermore, the volume element can easily be related to comoving distance $r(z)$ and the expansion rate $H(z)$ via $dV(z)/(d\Omega\, dz) = r^2(z)/H(z)$, and it is known exactly for a given cosmological model.

The sensitivity of cluster counts to dark energy arises – as in the case of weak lensing – from two factors:

- *geometry*, the term $dV(z)/(d\Omega\, dz)$ in Eq. (1.25) is the comoving volume element
- *growth of structure*, the mass function $n(z, M_{\rm min}(z))$ depends on the evolution of density perturbations.

The mass function's near-exponential dependence upon the power spectrum is at the root of the power of clusters to probe dark energy. More specifically, the mass function explicitly depends on the *amplitude of mass fluctuations* smoothed on some scale R

$$\sigma^2(R,z) = \int_0^\infty \Delta^2(k,z) \left(\frac{3j_1(kR)}{kR}\right)^2 d\ln k \tag{1.26}$$

where $\Delta^2(k,z)$ is the dimensionless power spectrum defined in Eq. (1.18), while R is traditionally taken to be $\sim 8\,{\rm h}^{-1}{\rm Mpc}$ at $z = 0$ and roughly corresponds to the typical size of a galaxy cluster. The term in angular parentheses is the Fourier transform of the top-hat window that averages out the perturbations over regions of radius R.

Systematic errors in cluster counts mainly concern uncertainty in how to convert from an observable quantity (X-ray light, gravitational lensing signal, etc) to the mass of a cluster. Current best estimates of mass are at the level of several tens of percent per cluster, and there is ongoing effort to find observable quantities, or combinations thereof, that are tightly correlated with mass.

The left panel of Fig. 1.9 shows the sensitivity to the dark energy equation-of-state parameter of the expected cluster counts for the South Pole Telescope and the Dark Energy Survey. At low to intermediate redshift, $z < 0.6$, the differences are dominated by the volume element; at higher redshift, the counts are most sensitive to the growth rate of perturbations. The right panel shows measurements of the mass function using recent X-ray observations of clusters.

Summary of principal probes. Figure 1.4 adopted from Amanullah *et al.* (2010), summarizes constraints in the Ω_M-Ω_Λ and Ω_M-w planes (the latter assuming

Table 1.1 Comparison of dark energy probes, adopted from Frieman *et al.* (2008). CDM refers to Cold Dark Matter paradigm, FoM is the Figure-of-Merit for dark energy surveys defined in the Dark Energy Task Force (DETF) report, while SZ refers to Sunyaev-Zeldovich effect.

Method	Strengths	Weaknesses	Systematics
WL	growth+geometry, Large FoM	CDM assumptions	Shear systematics, Photo-z
SN	pure geometry, mature	complex physics	evolution, dust extinction
BAO	pure geometry, low systematics	coarse-grained information	bias, non-linearity, redshift distortions
CL	growth+geometry, X-ray+SZ+optical	CDM assumptions	mass-observable, selection function

a flat universe) from CMB, BAO and SN Ia. In Table 1.1 we list the principal strengths and weaknesses of the four principal probes of DE. Control of systematic errors — observational, instrumental and theoretical — is crucial for these probes to realize their intrinsic power in constraining dark energy.

Role of the CMB. While the CMB provides precise cosmological constraints, by itself it has little power to probe dark energy. The reason is simple: the CMB provides a single snapshot of the Universe at a time when dark energy contributed a tiny part of the total energy density (a part in 10^9 if dark energy is the vacuum energy, or when $w = -1$). Nevertheless, the CMB plays a critical supporting role by determining other cosmological parameters, such as the spatial curvature and matter density, to high precision, thereby considerably strengthening the power of the methods discussed above. Essentially, what we get from the CMB is a *single* measurement of the angular diameter distance to recombination, $d_A(z \approx 1000)$ – therefore it provides a single very accurate measurement of the parameters Ω_M, $\Omega_{\rm DE}$ (if we do not assume a flat universe), and w (or $w(z)$ if we don't assume that the equation of state is constant). So, while the CMB alone suffers from degeneracy between the DE parameters, it is indispensable in breaking parameter degeneracies present in other cosmological probes; see Frieman *et al.* (2003) for more details. Data from the Planck CMB mission, launched in 2009, will therefore strongly complement those from dark energy surveys.

Secondary probes. There are a number of secondary probes of dark energy; here we review some of them.

- The Integrated Sachs-Wolfe (ISW) effect provided a confirmation of cosmic acceleration. ISW impacts the large-angle structure of the CMB anisotropy, but low-ℓ multipoles are subject to large cosmic variance, limiting the power of this probe. Nevertheless, ISW is of interest because it is able to reveal the imprint of large-scale dark-energy perturbations [Hu and Scranton (2004)].

- Gravitational radiation from inspiraling binary neutron stars or black holes can, if detected in the future, serve as "standard sirens" to measure absolute distances [Holz and Hughes (2005)]. If their redshifts can be determined, then they could be used to probe dark energy through the Hubble diagram [Dalal *et al.* (2006)].
- Long-duration gamma-ray bursts have been proposed as standardizable candles [Schaefer (2003)], but their utility as cosmological distance indicators that could be competitive with or complementary to SN Ia has yet to be established.
- The optical depth for strong gravitational lensing (multiple imaging) of QSOs or radio sources has been proposed and used to provide independent evidence for dark energy, though these measurements depend on modeling the density profiles of lens galaxies.
- The redshift drift effect (also known as the Sandage-Loeb effect [Sandage (1962); Loeb (1998)]) – the redshift change of an object measured using extremely high-resolution spectroscopy over a period of 10 years or more – may some day be useful in constraining the expansion history at higher redshift, $2 \lesssim z \lesssim 5$ [Corasaniti *et al.* (2007)].
- Polarization measurements from distant galaxy clusters – which probe the quadrupole of the CMB radiation at the epoch when the cluster light was emitted, and therefore the gravitational potential at that epoch – in principle provide a sensitive probe of the growth function and hence dark energy [Cooray *et al.* (2004)].
- The relative ages of galaxies at different redshifts, if they can be determined reliably, provide a measurement of dz/dt and, from

$$t(z) = \int_0^{t(z)} dt' = \int_z^\infty \frac{dz'}{(1+z')H(z')}, \tag{1.27}$$

measure the expansion history directly [Jimenez and Loeb (2002)].

1.5 The accelerating universe: summary

There are the five important things to know about dark energy:

(1) Dark energy has negative pressure. It can be described with its energy density relative to critical today $\Omega_{\rm DE}$, and equation of state $w \equiv p_{\rm DE}/\rho_{\rm DE}$; the cosmological constant (or vacuum energy) has $w = -1$ precisely and at all times. More general explanations for dark energy may have constant or time dependent equation of state. Assuming constant w, current constraints roughly give $w \approx -1 \pm 0.1$. Measuring the equation of state (and its time dependence) may help understand the nature of dark energy, and is a key goal of modern cosmology.

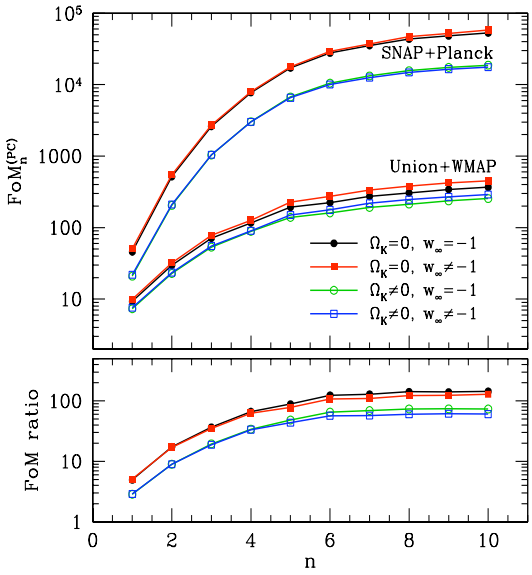

Fig. 1.10 Current and future figures of merit (FoM) for dark energy surveys, based on the principal-component (PC) based FoM from Eq. (1.17). *Top panel:* PC figures of merit $\mathrm{FoM}_n^{(\mathrm{PC})}$ with forecasted uncertainties for a combination of planned and ongoing space telescopes SNAP(SN)+Planck and with measured uncertainties for already completed surveys Union+WMAP. *Bottom panel:* Ratios of $\mathrm{FoM}_n^{(\mathrm{PC})}$ forecasts to current values. In both panels, point types indicate different quintessence model classes: flat (solid points) or non-flat (open points), either with (squares) or without (circles) early dark energy. Adopted from Mortonson *et al.* (2010).

(2) The accelerating universe quenches gravitational collapse of large structures and suppresses the growth of density perturbation: whenever dark energy dominates, structures do not grow, essentially because the expansion is too rapid.
(3) Dark energy comes to dominate the density of the universe only recently, at $z \lesssim 1$. At earlier epochs, dark energy density is small relative to matter density.
(4) Dark energy is spatially smooth. It affects both the geometry (that is, distances in the universe) and the growth of structure (that is, clustering and abundance of galaxies and clusters of galaxies).
(5) Dark energy can be probed using a variety of cosmological probes that measure geometry (i.e. the expansion history of the universe) and the growth of structure. Control of systematic errors in these cosmological probes is key to their success in measuring the properties of dark energy.

Acknowledgments

I thank Bob Kirshner, Eric Linder and Adam Riess for many useful comments on an earlier version of this manuscript, and to Josh Frieman and Michael Turner for collaboration on an earlier review [Frieman *et al.* (2008)] that helped me organize thoughts about dark energy. I am supported by DOE OJI grant under contract DE-FG02-95ER40899, NSF under contract AST-0807564, and NASA under contract NNX09AC89G.

Bibliography

Albrecht, A., Bernstein, G., Cahn, R., Freedman, W. L., Hewitt, J., Hu, W., Huth, J., Kamionkowski, M., Kolb, E. W., Knox, L., Mather, J. C., Staggs, S. and Suntzeff, N. B. (2006). Report of the Dark Energy Task Force, *astro-ph/0609591* .

Amanullah, R. *et al.* (2010). Spectra and Light Curves of Six Type Ia Supernovae at $0.511 < z < 1.12$ and the Union2 Compilation, *Astrophys. J.* **716**, pp. 712–738.

Astier, P. *et al.* (2006). The supernova legacy survey: Measurement of ω_m, ω_λ and w from the first year data set, *Astron. and Astroph.* **447**, pp. 31–48.

Baade, W. (1938). No. 600. The absolute photographic magnitude of supernovae. *Contributions from the Mount Wilson Observatory / Carnegie Institution of Washington* **600**, pp. 1–20.

Baade, W. and Zwicky, F. (1934). On Super-novae, *Proceedings of the National Academy of Science* **20**, pp. 254–259.

Bartelmann, M. and Schneider, P. (2001). Weak Gravitational Lensing, *Phys. Rept.* **340**, pp. 291–472.

Bartlett, J. G., Blanchard, A., Silk, J. and Turner, M. S. (1995). The Case for a Hubble constant of $30\mathrm{kms}^{-1}\mathrm{Mpc}^{-1}$, *Science* **267**, pp. 980–983.

Colgate, S. A. (1979). Supernovae as a standard candle for cosmology, *ApJ* **232**, pp. 404–408.

Conley, A. *et al.* (2008). SiFTO: An Empirical Method for Fitting SN Ia Light Curves, *ApJ* **681**, pp. 482–498.

Cooray, A., Huterer, D. and Baumann, D. (2004). Growth rate of large scale structure as a powerful probe of dark energy, *Phys. Rev.* **D69**, p. 027301.

Cooray, A. R. and Huterer, D. (1999). Gravitational lensing as a probe of quintessence, *ApJ* **513**, pp. L95–L98.

Corasaniti, P.-S., Huterer, D. and Melchiorri, A. (2007). Exploring the dark energy redshift desert with the sandage-loeb test, *Phys. Rev.* **D75**, p. 062001.

Dalal, N., Holz, D. E., Hughes, S. A. and Jain, B. (2006). Short GRB and binary black hole standard sirens as a probe of dark energy, *Phys. Rev. D* **74**, 6, p. 063006.

de Putter, R. and Linder, E. V. (2008). To Bin or Not To Bin: Decorrelating the Cosmic Equation of State, *Astropart. Phys.* **29**, p. 424.

Eisenstein, D. J. (2005). Dark energy and cosmic sound [review article], *New Ast. Rev.* **49**, pp. 360–365.

Eisenstein, D. J. *et al.* (2005). Detection of the baryon acoustic peak in the large-scale correlation function of sdss luminous red galaxies, *ApJ* **633**, pp. 560–574.

Frieman, J., Turner, M. and Huterer, D. (2008). Dark Energy and the Accelerating Universe, *Ann. Rev. Astron. Astrophys.* **46**, pp. 385–432.

Frieman, J. A., Huterer, D., Linder, E. V. and Turner, M. S. (2003). Probing dark energy with supernovae: Exploiting complementarity with the cosmic microwave background, *Phys. Rev. D* **67**, 8, p. 083505.

Garnavich, P. M. *et al.* (1998). Constraints on Cosmological Models from Hubble Space Telescope Observations of High-z Supernovae, *Astrophys. J.* **493**, pp. L53–57.

Guth, A. H. (1981). The inflationary universe: A possible solution to the horizon and flatness problems, *Phys. Rev.* **D23**, pp. 347–356.

Guy, J. *et al.* (2007). SALT2: using distant supernovae to improve the use of type Ia supernovae as distance indicators, *Astron. and Astroph.* **466**, pp. 11–21.

Hamuy, M. *et al.* (1996). BVRI Light Curves for 29 Type IA Supernovae, *A.J.* **112**, p. 2408.

Hicken, M. *et al.* (2009). Improved Dark Energy Constraints from ˜100 New CfA Supernova Type Ia Light Curves, *ApJ* **700**, pp. 1097–1140.

Hoekstra, H. and Jain, B. (2008). Weak Gravitational Lensing and Its Cosmological Applications, *Annual Review of Nuclear and Particle Science* **58**, pp. 99–123.

Holsclaw, T., Alam, U., Sanso, B., Lee, H., Heitmann, K. *et al.* (2010). Nonparametric Reconstruction of the Dark Energy Equation of State, *Phys.Rev.* **D82**, p. 103502.

Holz, D. E. and Hughes, S. A. (2005). Using gravitational-wave standard sirens, *ApJ* **629**, pp. 15–22.

Holz, D. E. and Linder, E. V. (2005). Safety in numbers: Gravitational lensing degradation of the luminosity distance-redshift relation, *ApJ* **631**, pp. 678–688.

Hu, W. and Scranton, R. (2004). Measuring dark energy clustering with cmb-galaxy correlations, *Phys. Rev.* **D70**, p. 123002.

Huterer, D. (2010). Weak lensing, dark matter and dark energy, *Gen. Rel. Grav.* **42**, pp. 2177–2195.

Huterer, D. and Cooray, A. (2005). Uncorrelated estimates of dark energy evolution, *Phys. Rev.* **D71**, p. 023506.

Huterer, D. and Starkman, G. (2003). Parameterization of dark-energy properties: A principal- component approach, *Phys. Rev. Lett.* **90**, p. 031301.

Huterer, D. and Turner, M. S. (1999). Prospects for probing the dark energy via supernova distance measurements, *Phys.Rev.* **D60**, p. 081301.

Huterer, D. and Turner, M. S. (2001). Probing the dark energy: Methods and strategies, *Phys. Rev.* **D64**, p. 123527.

Jha, S., Riess, A. G. and Kirshner, R. P. (2007). Improved Distances to Type Ia Supernovae with Multicolor Light-Curve Shapes: MLCS2k2, *ApJ* **659**, pp. 122–148.

Jimenez, R. and Loeb, A. (2002). Constraining cosmological parameters based on relative galaxy ages, *ApJ* **573**, pp. 37–42.

Kessler, R. *et al.* (2009). First-year Sloan Digital Sky Survey-II (SDSS-II) Supernova Results: Hubble Diagram and Cosmological Parameters, *Astrophys. J. Suppl.* **185**, pp. 32–84.

Kim, A. (2008). Stretched and non-stretched B-band supernova light curves, *LBNL Report LBNL-56164* .

Kirshner, R. P. (2002). *The extravagant universe : exploding stars, dark energy and the accelerating cosmos.*

Kirshner, R. P. (2009). Foundations of Supernova Cosmology, *arXiv:0910.0257* .

Knop, R. A. *et al.* (2003). New Constraints on Ω_M, Ω_Λ, and w from an Independent Set of Eleven High-Redshift Supernovae Observed with HST, *Astrophys. J.* **598**, p. 102.

Kowal, C. T. (1968). Absolute magnitudes of supernovae. *A.J.* **73**, pp. 1021–1024.

Linder, E. V. (2003). Exploring the expansion history of the universe, *Phys. Rev. Lett.* **90**, p. 091301.

Linder, E. V. (2010). Frontiers of Dark Energy, *arXiv:1009.1411* .

Loeb, A. (1998). Direct Measurement of Cosmological Parameters from the Cosmic Deceleration of Extragalactic Objects, *ApJL* **499**, p. L111.

Mohr, J. J. (2005). Cluster Survey Studies of the Dark Energy, in S. C. Wolff and T. R. Lauer (eds.), *Observing Dark Energy*, *Astronomical Society of the Pacific Conference Series*, Vol. 339, p. 140.

Mortonson, M. J., Huterer, D. and Hu, W. (2010). Figures of merit for present and future dark energy probes, *Phys. Rev. D* **82**, 6, p. 063004.

Nakamura, T. and Chiba, T. (1999). Determining the equation of state of the expanding universe: Inverse problem in cosmology, *Mon. Not. Roy. Astron. Soc.* **306**, pp. 696–700.

Norgaard-Nielsen, H. U., Hansen, L., Jorgensen, H. E., Aragon Salamanca, A. and Ellis, R. S. (1989). The discovery of a type IA supernova at a redshift of 0.31, *Nature* **339**, pp. 523–525.

Peebles, P. J. E. (1984). Tests of cosmological models constrained by inflation, *ApJ* **284**, pp. 439–444.

Percival, W. J. *et al.* (2010). Baryon Acoustic Oscillations in the Sloan Digital Sky Survey Data Release 7 Galaxy Sample, *Mon. Not. Roy. Astron. Soc.* **401**, pp. 2148–2168.

Perlmutter, S. and Schmidt, B. P. (2003). Measuring Cosmology with Supernovae, in K. Weiler (ed.), *Supernovae and Gamma-Ray Bursters*, *Lecture Notes in Physics, Berlin Springer Verlag*, Vol. 598, pp. 195–217.

Perlmutter, S. *et al.* (1997). Measurements of the Cosmological Parameters Omega and Lambda from the First Seven Supernovae at $z \geq 0.35$, *ApJ* **483**, p. 565.

Perlmutter, S. *et al.* (1998). Discovery of a Supernova Explosion at Half the Age of the Universe and its Cosmological Implications, *Nature* **391**, pp. 51–54.

Perlmutter, S. *et al.* (1999). Measurements of Omega and Lambda from 42 High-Redshift Supernovae, *Astrophys. J.* **517**, pp. 565–586.

Phillips, M. M. (1993). The absolute magnitudes of Type Ia supernovae, *ApJL* **413**, pp. L105–L108.

Press, W. H. and Schechter, P. (1974). Formation of galaxies and clusters of galaxies by selfsimilar gravitational condensation, *Astrophys. J.* **187**, pp. 425–438.

Riess, A. G., Press, W. H. and Kirshner, R. P. (1996a). A Precise Distance Indicator: Type IA Supernova Multicolor Light-Curve Shapes, *ApJ* **473**, p. 88.

Riess, A. G., Press, W. H. and Kirshner, R. P. (1996b). Is the Dust Obscuring Supernovae in Distant Galaxies the Same as Dust in the Milky Way? *ApJ* **473**, p. 588.

Riess, A. G. *et al.* (1998). Observational Evidence from Supernovae for an Accelerating Universe and a Cosmological Constant, *A.J.* **116**, pp. 1009–1038.

Riess, A. G. *et al.* (2004). Type ia supernova discoveries at $z > 1$ from the hubble space telescope: Evidence for past deceleration and constraints on dark energy evolution, *ApJ* **607**, pp. 665–687.

Riess, A. G. *et al.* (2007). New Hubble Space Telescope Discoveries of Type Ia Supernovae at $z \geq 1$: Narrowing Constraints on the Early Behavior of Dark Energy, *ApJ* **659**, pp. 98–121.

Sahni, V. and Starobinsky, A. (2006). Reconstructing Dark Energy, *astro-ph/0610026* .

Sandage, A. (1962). The Change of Redshift and Apparent Luminosity of Galaxies due to the Deceleration of Selected Expanding Universes. *ApJ* **136**, pp. 319–333.

Schaefer, B. E. (2003). Gamma-Ray Burst Hubble Diagram to z=4.5, *ApJL* **583**, pp. L67–L70.

Starobinsky, A. A. (1998). How to determine an effective potential for a variable cosmological term, *JETP Lett.* **68**, pp. 757–763.

Takada, M. and Jain, B. (2004). Cosmological parameters from lensing power spectrum and bispectrum tomography, *Mon. Not. Roy. Astron. Soc.* **348**, p. 897.

Tinker, J. L. *et al.* (2008). Toward a halo mass function for precision cosmology: the limits of universality, *Astrophys. J.* **688**, pp. 709–728.

Turner, M. S., Steigman, G. and Krauss, L. M. (1984). Flatness of the universe - Reconciling theoretical prejudices with observational data, *Phys. Rev. Lett.* **52**, pp. 2090–2093.

Vikhlinin, A. *et al.* (2009). Chandra Cluster Cosmology Project III: Cosmological Parameter Constraints, *Astrophys. J.* **692**, pp. 1060–1074.

Wang, Y. and Mukherjee, P. (2004). Model-independent constraints on dark energy density from flux-averaging analysis of type ia supernova data, *ApJ* **606**, pp. 654–663.

Wang, Y. and Tegmark, M. (2005). Uncorrelated measurements of the cosmic expansion history and dark energy from supernovae, *Phys. Rev.* **D71**, p. 103513.

Weller, J. and Albrecht, A. (2002). Future supernovae observations as a probe of dark energy, *Phys. Rev.* **D65**, p. 103512.

Wood-Vasey, W. M. *et al.* (2007). Observational Constraints on the Nature of the Dark Energy: First Cosmological Results from the ESSENCE Supernova Survey, *Astrophys. J.* **666**, pp. 694–715.